Biomimetic toughening design of 3D-printed polymeric structures
Enhancing toughness through sacrificial bonds and hidden lengths

Xu, Z.; Tao, R.; Masania, K.; Teixeira De Freitas, S.

DOI
10.1016/j.matdes.2024.113361

Publication date
2024

Document Version
Final published version

Published in
Materials & Design

Citation (APA)
Xu, Z., Tao, R., Masania, K., & Teixeira De Freitas, S. (2024). Biomimetic toughening design of 3D-printed polymeric structures: Enhancing toughness through sacrificial bonds and hidden lengths. *Materials & Design*, *247*, Article 113361. https://doi.org/10.1016/j.matdes.2024.113361

Materials & Design 247 (2024) 113361

Contents lists available at ScienceDirect

Materials & Design

journal homepage: www.elsevier.com/locate/matdes

Biomimetic toughening design of 3D-printed polymeric structures: Enhancing toughness through sacrificial bonds and hidden lengths

Zhiyuan Xu [a], Ran Tao [a], Kunal Masania [b,*], Sofia Teixeira de Freitas [a,c,*]

[a] Faculty of Aerospace Engineering, Delft University of Technology, Delft 2629 HS, Netherlands
[b] Shaping Matter Lab, Faculty of Aerospace Engineering, Delft University of Technology, Delft 2629 HS, Netherlands
[c] IDMEC, Instituto Superior Técnico, Universidade de Lisboa, Lisboa, Portugal

ARTICLE INFO

Dataset link: https://doi.org/10.4121/5df63ddf-8630-4a05-b446-75dd9abe3e24

Keywords:
Biomimetic materials
Sacrificial bonds
Hidden lengths
Toughness

ABSTRACT

Spider silk is known for its excellent strength and fracture resistance properties due to its molecular design structure, characterized by sacrificial bonds and hidden lengths. These structures have inspired reinforcements of synthetic polymer materials to enhance toughness. In this study, we mimic these natural toughening mechanisms by designing and manufacturing 3D-printed polymeric structures incorporating overlapping curls consisting of coiling fiber with sacrificial bonds and hidden lengths. Utilizing the liquid rope coiling effect, we manufactured overlapping curls using three polymers: polylactic acid (PLA), liquid crystal polymer (LCP), and polyamide 6 (PA6). Uniaxial tensile tests were performed to characterize the mechanical properties of overlapping curl as a function of geometries, post-treatments, and material constitutive parameters. Our results show that single-sided overlapping curls can fully unfold while double-sided curls are prone to premature failure. Heat-pressure post-treatment was found to significantly increase the load-capacity of the sacrificial bonds by up to 77 % due to increased contact area. However, the defects introduced in the fibre after the break of the sacrificial bonds, make the structure more susceptible to premature failure, limit the complete unfolding of the hidden length, and lead to a decrease up to 67 % of the toughness. To guarantee the complete unfolding of the hidden lengths and improve the toughness, we demonstrate that selecting a polymer material with either high fracture strength (e.g., LCP, 311 MPa) or high fracture strain (e.g., PA6, >2) is crucial, and increase toughness up to 32 % and 46 %, respectively.

1. Introduction

With the appeal to sustainability requirements in engineering, robust and eco-friendly load-bearing materials are in high demand. Natural materials, with billions of years of evolution, provide plenty of sophisticated and hierarchical material structures that exhibit strength and fracture resistance at low environmental costs, for example, spider silk [1,2], bone [3,4], and nacre [5,6]. These hierarchical structures have inspired composite material design to improve its intrinsic lower properties such as toughness [7,8] and impact performance [9]. One of the stiffening and toughening mechanisms contributing to the superior mechanical properties is the overlapping curl (OC) structure which consists of a coiling fiber with sacrificial bonds and hidden lengths. This structure allows, upon stretching, for the break of the weak sacrificial bonds and the release of hidden lengths, e.g., the β-sheet in spider silk (Fig. 1(a)), providing a residual stiffness and strength that retards complete fracture. Various applications have adopted this mechanism to develop high-performance biomimetic materials, such as hydrogels [10,11] at a microscopic scale, elastomers [12–14] and composites [15,16] at a macroscopic scale.

In recent years, progress in engineering materials and processes has driven the development of 3D-printing technology and allowed new applications such as shape memory structures [17], composite materials [18,19], and 4D printing [20,21]. The macroscopic overlapping curl structures can also be fabricated by 3D-printing processes such as melt electrowriting [22,23], directing ink writing [24,25], and fused filament fabrication [26–28]. Among them, fused filament fabrication is a mature and widely adopted approach to produce complex geometries [29,30] with a wide range of engineering materials, including thermoplastics [26], glass [31], and carbon fiber reinforced composites [32]. Based on the liquid rope coiling (LRC) effect [33,34], where the coiling of a viscous fluid occurs through buckling during falling from

* Corresponding authors.
E-mail address: s.teixeiradefreitas@tudelft.nl (S. Teixeira de Freitas).

https://doi.org/10.1016/j.matdes.2024.113361
Received 20 August 2024; Received in revised form 1 October 2024; Accepted 3 October 2024
Available online 17 October 2024

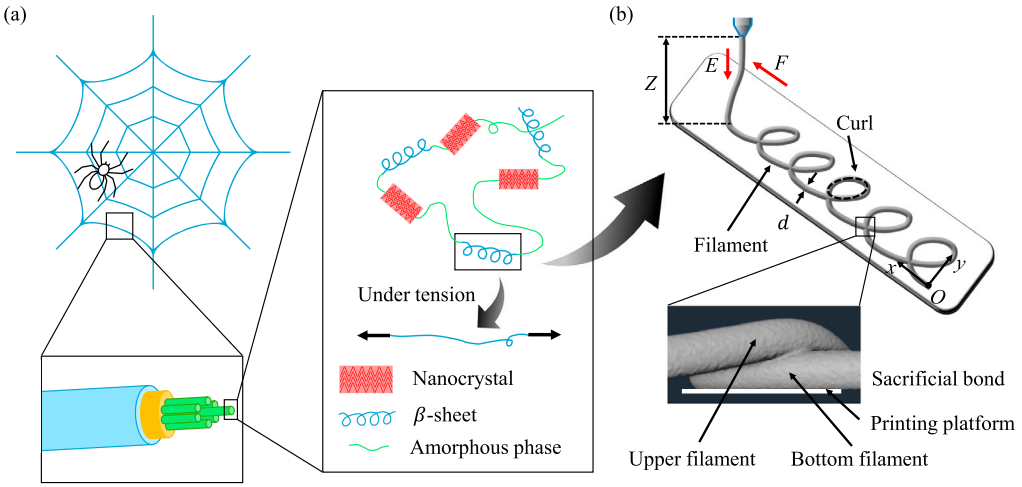

Fig. 1. (a) Schematic of spider web and spider silk structure. Adapted from original references [14,36,37]. (b) Schematic of the overlapping curl structure manufacturing process. The sacrificial bond is formed by the upper filament contacting the bottom filament. The curl is the ellipse shape of the overlapping curl filament closed by sacrificial bonds.

a sufficient height, fused filament fabrication with LRC has been used to fabricate the OC structures in an off-the-shelf, rapid, and cost-effective way. Under the foundation of the experimental and analytical investigations [24,28,35], by a proper selection of printing parameters, such as nozzle moving speed, filament extrusion value, deposition height, nozzle oscillation, etc., a rich variety of periodic overlapping curl patterns could be generated.

Works have combined 3D-printing and polymers to design the OC structures and desired mechanical properties [14,25–27]. Passieux et al. [25] tailored the mechanical properties of polylactic acid OC by various patterns through adjusting printing parameters. The results indicated that the toughness improvement is directly related to the hidden length extension. A complete release of hidden lengths led to a maximal 200 % toughness enhancement compared to straight lines. Subsequently, Zou et al. [26] investigated the mechanics behind premature failures of OC before a complete extension of hidden lengths, attributing them to local bending and torsion stresses during hidden length unfolding. Cellular or foam structures based on overlapping curls were also fabricated with tunable stiffness. Using silicone, Ma et al. [28] fabricated silicone cubes with OC pattern line by line, layer by layer. As the cubes are compressed, the touching and densifying between the OC layers induce the variable larger nonlinear deformation according to the unit pattern of OC. Willemstein et al. [27] designed the porosity structure with the unit cell of coils and programmed the density, stiffness, and energy dissipation. Significant variations were achieved, including an 89 % reduction in density and a 246-fold increase in compression modulus. Both examples provide new ideas for variable stiffness and functionalized materials by using OC structure. Previous studies mainly focused on the as-printed curls properties and are limited to non-structural material (low strength and low stiffness - Young's modulus 3∼2500 MPa, tensile strength 1∼60 MPa). However, research on how to improve the overlapping curl toughness after printing and the influence of the material properties is still limited.

This paper seeks to address this research gap in order to explore these bio-inspired structures to their full potential to improve the toughness of structural materials, such as composite material or bio-based polymer resin. To accomplish this, heat and pressure post-treatments have been applied to improve the sacrificial bond load-capacity using three distinct polymer materials, polylactic acid as the reference (Young's modulus∼2588 MPa, tensile strength∼58 MPa), liquid crystal polymer as high strength and high stiffness material (Young's modulus∼5820 MPa, tensile strength∼311 MPa), and polyamide as a very ductile material (elongation∼200 %).

Table 1
3D-printing and post-treatment temperatures for the overlapping curl structures.

Material	PLA	LCP	PA6
Melting temperature (°C)	210 [39]	280 [40]	260 [41]
Glass transition temperature (°C)	60 [42]	∼120 [43]	72 [41]
Nozzle temperature (°C)	275	360	275
Platform temperature (°C)	80	100	80
Post-treatment temperature (°C)	80	270 [44]	80

2. Materials and methods

2.1. Materials

Three commercial polymer materials were used to manufacture overlapping curl structures. Polylactic acid filament (PLA, ReForm™ - rPLA) was purchased from Formfutura BV company (Nijmegen, Netherlands). The liquid crystal polymer (LCP, Vectra A950) was purchased from NematX AG (Zürich, Switzerland). Polyamide filament with major Polyamide 6 content (PA6, F3 PA Pure Pro) was obtained from Fiberthree GmbH company (Darmstadt, Germany). The melting and glass transition temperatures of these materials from datasheets and references are listed in Table 1.

2.2. Manufacturing of overlapping curl

Fig. 1(b) shows the fused filament fabrication 3D-printing manufacturing process of overlapping curl consisting of coiling fiber with sacrificial bonds and hidden length by adopting the LRC effect. A custom-written g-code, combining the nozzle horizontal moving speed F, filament extrusion value E, and the nozzle height Z was sent to a commercially available 3D printer (Prusa i3 MK3S+). Two nozzles with different diameters: 0.4 mm and 0.8 mm were used to print the curls with different filament diameters d. After the extruded molten polymer filament solidified in ambient air, the weakly fused sacrificial bonds were formed by the upper filament contacting the bottom filament. The printing temperatures and processing conditions are summarized in Table 1. To achieve a strong sacrificial bond, we set the printing temperature higher than the material melting temperature which kept the extruded filament in the melting state longer. The printing platform temperature was also set at a high value to reduce the heat loss due to the air heat radiation [38].

For each nozzle size (0.4 mm and 0.8 mm) and each printing material (PLA, LCP, and PA6), four overlapping curl topologies were manufactured: single (S) or double (D) directional curl, and curl size controlled

Table 2
3D-printing parameters and structures of PLA overlapping curl. Z: nozzle height, F: nozzle moving speed, and E: the filament extrusion value.

Nomenclature	Nozzle size (mm)	Orientation	Z (mm)	F (mm/min)	E (mm/min)	Resulting OC structure
PLA_0.4_S_Z10	0.4	Single	10	750	75	 5 mm
PLA_0.4_S_Z5	0.4	Single	5	750	75	 5 mm
PLA_0.4_D_Z10	0.4	Double	10	1000	60	 5 mm
PLA_0.4_D_Z5	0.4	Double	5	1000	60	 5 mm

by the two nozzle height 10 mm (Z10) and 5 mm (Z5). Table 2 summarizes the printing parameters used for the four topologies, for the example of PLA material using 0.4 mm size nozzle, presenting the nomenclature, 'Material_Nozzle size_Orientation_Nozzle height'. The filament diameter d of OC manufactured with a 0.4 mm nozzle is approximately 0.55 mm and 0.8 mm nozzle is approximately 0.88 mm. When printing the curl using PA6 with a nozzle size 0.8 mm, the printing process was unstable and a significant amount of air bubbles could be observed.[1] Therefore, this overlapping curl structure was not included in this work further.

2.3. Post-treatment on overlapping curl

With the aim to modify the sacrificial bonds load-capacity, two types of post-treatments were applied to the as-printed curl structures: heat and heat-pressure. The post-treatment temperatures for each material were carefully selected to avoid thermal degradation of the material [29] – see Table 1. In the heat treatment, the as-printed samples were put into a vacuum oven and heated for 6 hours. For the heat-pressure treatment, during the same heating process, metal plates with 3.2 N weight were placed on top of the OC samples to provide additional pressure at sacrificial bonds (5 samples in one heat-pressure treatment).

2.4. Contact area in sacrificial bonds

The macrostructure of OC was analyzed by X-ray computed tomography (X-ray CT, CoreTOM, TESCAN, Belgium). The X-ray source was powered by a voltage of 120 kV and a current density of 0.75 mA with 1920×1896 pixels silicon flat panel detector. The scanning consisted of 1440 images at a rate of 10.5 images/s with a voxel size of 25 μm. Once the 2D images were acquired, the 3D volume reconstruction was carried out on Panthera 1.4 software. 3D volumes were visualized through the commercial software Avizo (Avizo, Thermo Fisher Scientific, Massachusetts, USA). Post-mortem scanning electron microscopy (SEM, JSM-7500F, JEOL Co., Japan) was employed to visualize the fracture surface morphological characteristics of sacrificial bonds. An example of the fracture surface is given in Fig. 2(a) - right hand side photo.

In order to measure the contact area C_A in the sacrificial bonds, we utilized the X-ray CT to scan the geometry profile of the overlapping curl. To quantify the value of C_A, we adopted the discrete approximation method that splits the contact area into several small triangles and trapezoids and then sums the sub-areas up. The C_A was then determined as an approximation of the C_A shown in the SEM picture (Fig. 2(a)) by using the X-ray values for the contact length l_i and translated distance d_i between the two adjacent slice planes shown in Fig. 2(b). The expression for calculating C_A is,

$$C_A = \frac{1}{6}\sum_{i=1}^{5}(l_i)\cdot d_p \tag{1}$$

where d_p is the total distance between the 1st and 7th slice planes, i.e., $d_p = \sum_{i=1}^{6} d_i$. The accuracy of the proposed method is validated by a 3 % error when measuring the hypothetical ellipse area (resembling the shape of the contact area of the sacrificial bond) compared to the actual value.

2.5. Mechanical testing

Tensile tests were conducted using a universal Zwick loading frame to obtain the mechanical properties of overlapping curl samples with a 100 N loadcell. The loading was in displacement control at a rate of 5 mm/min and the displacement was measured with a mechanical extensometer. The experimental setup for overlapping curl testing is shown in Fig. 3. The OC sample was bonded to tabs with a step-wise shape to ensure that the loading axis aligns with the filament. The tabs were then clamped by the load frame grips to avoid sample damage at the grip location. At least five specimens of each OC structure were tested. In the Z10 specimens, the gauge length covered 6 curls, while in the Z5, covered 10 curls.

3. Results and discussion

3.1. Mechanical parameter definition

As shown in Fig. 4(a), the typical force-displacement curve starts from a rising load up to point **i** until the first sacrificial bond breaks followed by a load drop. As the load increases, the curl unfolds till a cusp forms at point **ii**, unravelling the hidden length of the curl. At this point, the cusp still contains some hidden length. Then, the OC initiates a straightening process again with a subsequent increase in the load up to the next load drop, as the second sacrificial bond breaks (point **iii**). The sacrificial bonds break one by one, resulting in a saw-tooth tensile curve. After all the sacrificial bonds break and curls unfold into cusps at point **iv**, the remaining hidden lengths in cusps start to further extend until the ultimate failure of the filament (point **v**). It should be noted that during hidden lengths unfolding, the filament in the curl first experiences bending and torsion loading [26]. After the hidden lengths totally

[1] With lower printing temperature, the air bubbles can be decreased but at the expense of weak sacrificial bonds which is not preferred.

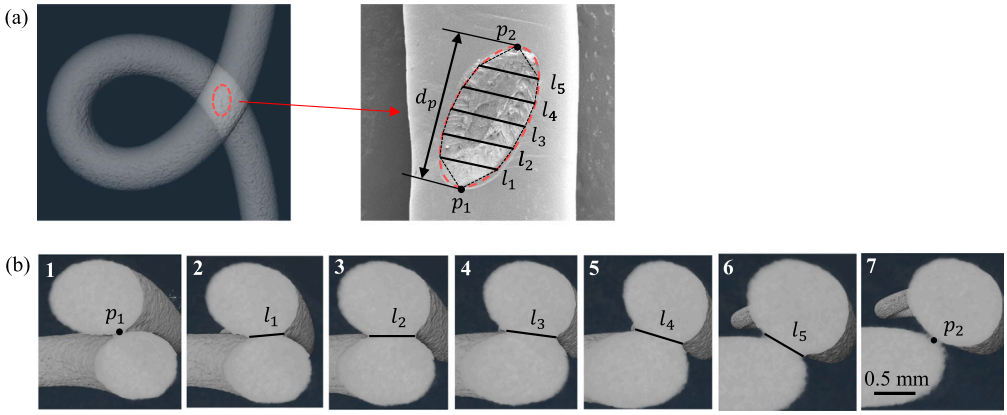

Fig. 2. (a) X-ray CT observation of sacrificial bond. The contact area in the sacrificial bond was outlined in SEM image. (b) The slice planes used to estimate the contact area.

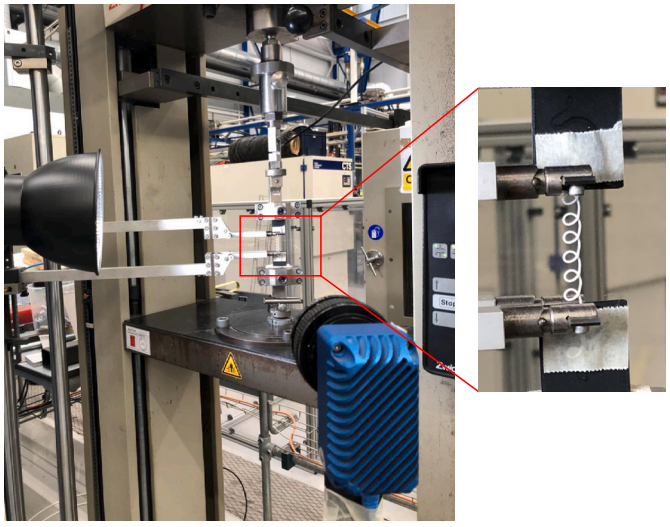

Fig. 3. Mechanical set-up for overlapping curl tensile test. The zoomed image highlights one testing OC sample.

unfold, the loading state changes to axial tension. To better quantify the mechanical properties of overlapping curl, we define some critical parameters as seen in Fig. 4(a):

- F_{sb}, sacrificial bond load-capacity: the force to break sacrificial bonds. We hypothesize that F_{sb} is related to the contact area C_A in the sacrificial bond;
- F_u, ultimate maximal load: the maximal force value right before the failure of OC filament. It is assumed that this value is only valid after at least one sacrificial bond breaks and the corresponding hidden length unfolds.
- p, the unfolding percentage of hidden length.

$$p = \frac{l_d}{(n-1) \times l_{hl}} \tag{2}$$

where l_d is the unfolding hidden lengths between the immediate break of the first and last sacrificial bonds, as indicated in Fig. 4(a). l_{hl} is the perimeter of each curl and is calculated by the measured average curl geometries in each tested overlapping curl sample. n is the number of broken sacrificial bonds in the sample: $n = 6$ for Z10 and $n = 10$ for Z5 samples.

- Δl: the maximal axial displacement upon ultimate filament failure.
- E_T, toughness: the ability to absorb energy during the OC tensile process. It is represented by the shaded area under the force-displacement curve per unit mass as follows [45]:

$$E_T = \frac{\int_0^{\Delta l} F dl}{m} \tag{3}$$

where m is the mass of tested sample.

3.2. Material constitutive properties

The polymer material constitutive properties were determined by testing the straight lines also fabricated with LRC effect through increasing F and decreasing E. The straight lines had the same cross-section diameter as the overlapping curl filament, except for the LCP straight line ($d = 0.75$ mm) whose diameter was smaller compared to the OC filament ($d = 0.88$ mm). We assume that the mechanical properties are constant in this small diameter variation. The testing setup for the straight line is the same as the overlapping curl (described in Section 2.5) with at least five straight lines tested for each material. Tensile tests were performed before and after heat treatment and the material constitutive properties are summarized in Table 3. We see that the LCP exhibits the highest Young's modulus (more than twice that of PLA and PA6), tensile and fracture strength (more than five times), and PA6 demonstrates extraordinarily high fracture strain compared with PLA and LCP (one to two orders of magnitude higher). In general, the heat treatment improved Young's modulus and tensile strength of the materials, due to enhanced molecular alignment, increased crystallinity, and the release of residual stress from fabrication [44,46–49].

3.3. Mechanical analysis of PLA overlapping curl

3.3.1. As-printed overlapping curl

To study the effect of the nozzle size, nozzle height, and curl's orientation on the tensile properties, the tensile results of these overlapping curl structures manufactured from PLA material were analyzed. Fig. 5(a) and 5(b) show the typical saw-tooth force-displacement curves of PLA single and double OC under axial load, respectively; however, they exhibit distinct failure responses.

From Fig. 5(a), in the single OC, all the sacrificial bonds break and the hidden lengths fully unfold until the ultimate filament failure. It can be seen that the samples printed with 0.4 mm nozzle size (PLA_0.4_S_Z10 and PLA_0.4_S_Z5) show a plateau after reaching the peak load corresponding to the necking observed during the tests. While the samples printed with the thicker nozzle (0.8 mm) show brittle failure after reaching F_u. This distinct behaviour might be due to size effects in the PLA material and non-uniform stress distribution in the cross-section of the filament, which was also observed in [25,26,50].

In contrast, the double OC (Fig. 5(b)) experiences premature failure where the filament fails before all the sacrificial bonds break and hidden lengths unfold, demonstrating a truncated elongation. Especially, the thicker double ones (PLA_0.8_D_Z10, Z5) fail ultimately before any

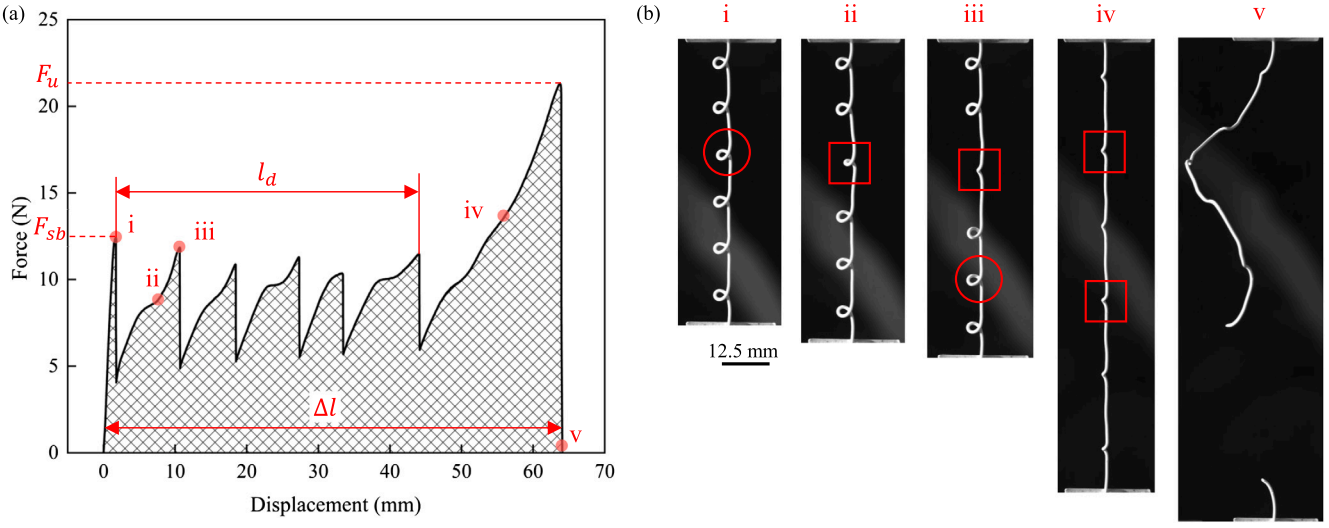

Fig. 4. (a) Schematic for overlapping curl force-displacement curve. (b) The snapshots of the sample deformation during the tensile test process. The red circle denotes the position of the broken sacrificial bond. The rectangle shows the cusp in the curl after the hidden length unfolds.

Table 3
Mechanical properties of straight lines printing materials before and after heat treatment.

Material	PLA		LCP		PA6	
	as-printed	heat	as-printed	heat	as-printed	heat
Young's modulus (MPa)	2588±81	2643±112	5820±195	7089±232	2064±97	2885±357
Tensile strength (MPa)[a]	58±0.74	67±4.4	311±20	359±21	59±0.71	68±1.7
Fracture strength (MPa)[b]	54±1.8	59±8.8	311±20	359±21	47±0.97	58±2.5
Fracture strain (-)	0.033±0.002	0.037±0.0014	0.15±0.014	0.16±0.025	>2	>2

[a] Tensile strength is the maximal stress in the stress-strain curve.
[b] Fracture strength is stress where the straight line fractures.

sacrificial bond breaks. Such a premature failure may stem from the manufacturing stage. In Fig. 5(c), the patterns of single and double OC are predicted by the geometric model of liquid rope coiling effect [35], and the extruded filament movement periodic orbits are also described. In the single OC, the extruded filament moves in a self-similar manner, maintaining a consistent orbit curvature as it is deposited onto the printing platform. While in double OC, the extruded filament experiences much larger orbit curvature variations which leads to possible more stress concentration and premature failure during loading in comparison with the single counterpart.

Looking into the initial part of these force-displacement curves, we find that the initial stiffness is different among the single and double overlapping curl. The single OC shows similar initial stiffness regardless of the nozzle size and curl's size (Fig. 5(a)), while there is a considerable variation in the initial stiffness of the double OC, see Fig. 5(b) in the zoomed box. The stiffness in 0.8 mm double OC is higher than the 0.4 mm counterpart because of its thicker filament diameter. Besides, PLA_0.8_D_Z5 has higher stiffness than PLA_0.8_D_Z10. In order to understand this phenomenon, Fig. 5(d) plots the geometric curvature between the two adjacent sacrificial bonds. When overlapping curl is under tension, before the first sacrificial bond breaks, a higher force is needed to straighten the filament between sacrificial bonds of PLA_0.8_D_Z5 due to its larger curvature. Therefore, the orbit curvature and geometric curvature of OC demonstrate critical effects on its mechanical response, such as causing premature failure and increasing initial stiffness.

Fig. 6 summarizes F_{sb} and F_u values of each overlapping curl structure. For a given nozzle size, the F_{sb} is almost the same regardless of the nozzle height (Z) and curl's orientation (S or D). However, the F_{sb} and F_u for 0.8 mm nozzle size are higher than the corresponding 0.4 mm - see Fig. 6(a). The filament cross-sectional area is larger in 0.8 mm than in 0.4 mm which leads to the higher F_u. To further understand the factors that determine F_{sb}, the contact area C_A in the sacrificial bond was calculated by Equation (1) and plotted in Fig. 6. Based on the X-ray CT observation, PLA_0.8_S_Z10 has a larger C_A value, leading to the larger F_{sb} than PLA_0.4_S_Z10. However, although the C_A in PLA_0.8_S_Z10 is larger than PLA_0.8_S_Z5, the latter exhibits a higher F_{sb}. This indicates that F_{sb} depends not only on the contact area but also on the filament's remaining temperature when the sacrificial bond forms. Since the nozzle height is shorter in PLA_0.8_S_Z5, the temperature in the extruded filament is still high because of the shorter cooling time before the upper and bottom filaments contact each other. Therefore, the upper and bottom filaments contain more melted content material, which results in a stronger sacrificial bond. This phenomenon compensates for F_{sb} in PLA_0.8_S_Z5, despite the smaller C_A. The same reasoning is valid when comparing PLA_0.8_S_Z5 with PLA_0.4_S_Z10 and PLA_0.4_S_Z5, where a larger nozzle is more effective in maintaining the temperature of the extruded filament due to the increased extrusion volume of molten material [38].

In Fig. 6(b), the C_A of PLA_0.4_D_Z10 has a larger standard deviation due to the noticeable difference in the curls' shape inherent to this double OC topology. As observed in Fig. 6(b), PLA_0.8_D_Z10 and PLA_0.8_D_Z5 show premature failures, with no sacrificial bond break, limiting the data. It is clear from Fig. 6 that, F_{sb} is always smaller than the corresponding F_u. To improve toughness of the overlapping curl structures, ideally, F_{sb} would reach as close as possible to the value of F_u. Therefore, we seek to increase F_{sb} through post-treatments applied to the overlapping curl.

3.3.2. Post-treated overlapping curl

Fig. 7 plots the force-displacement curves of the PLA overlapping curls with single orientation (S) before and after post-treatments. In general, after heat treatment, F_{sb} stays the same and F_u presents an increase but with less unravelling of hidden length. The tensile strength of PLA material increases after heat which leads to a higher F_u in

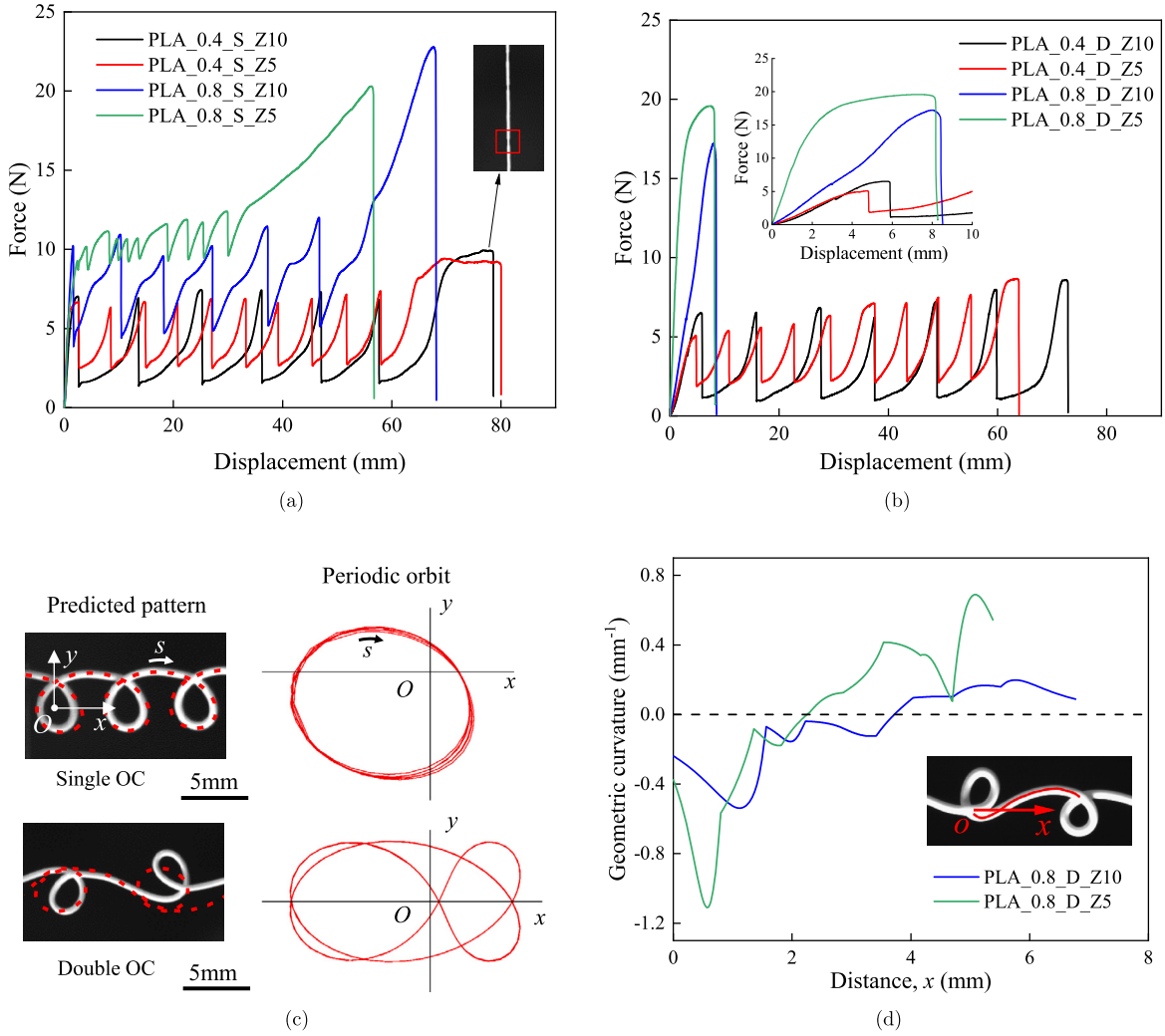

Fig. 5. (a) Representative force-displacement tensile curves of PLA single overlapping curl. The red rectangle in the insert picture shows the necking of filament before ultimate failure. (b) Representative force-displacement tensile curves of PLA double OC and the insert is the zoomed curve. (c) Comparison of the predicted patterns (red dashed line) and the extruded filament movement periodic orbits (red line) of PLA single and double OC based on geometric model [35]. (d) The geometric curvature between two adjacent sacrificial bonds on PLA 0.8 mm double OC. The insert picture highlights the x-axis location of the graph of the overlapping curl geometry.

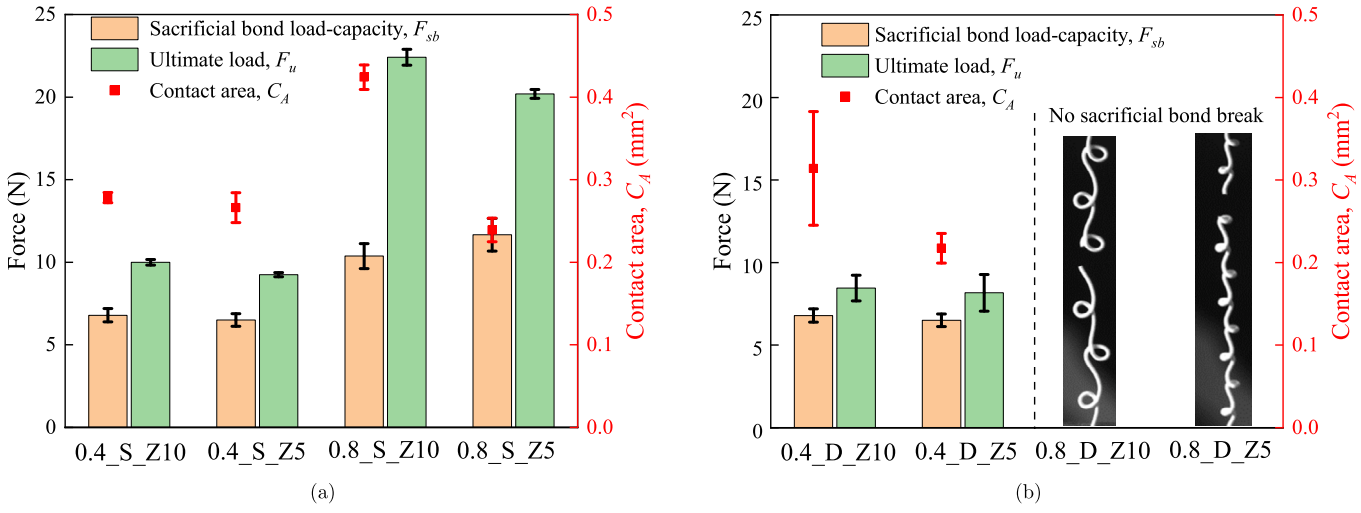

Fig. 6. F_{sb}, F_u, and C_A in (a) PLA single and (b) PLA double overlapping curl. The insets are the fracture pieces of thick 0.8 mm double overlapping curl.

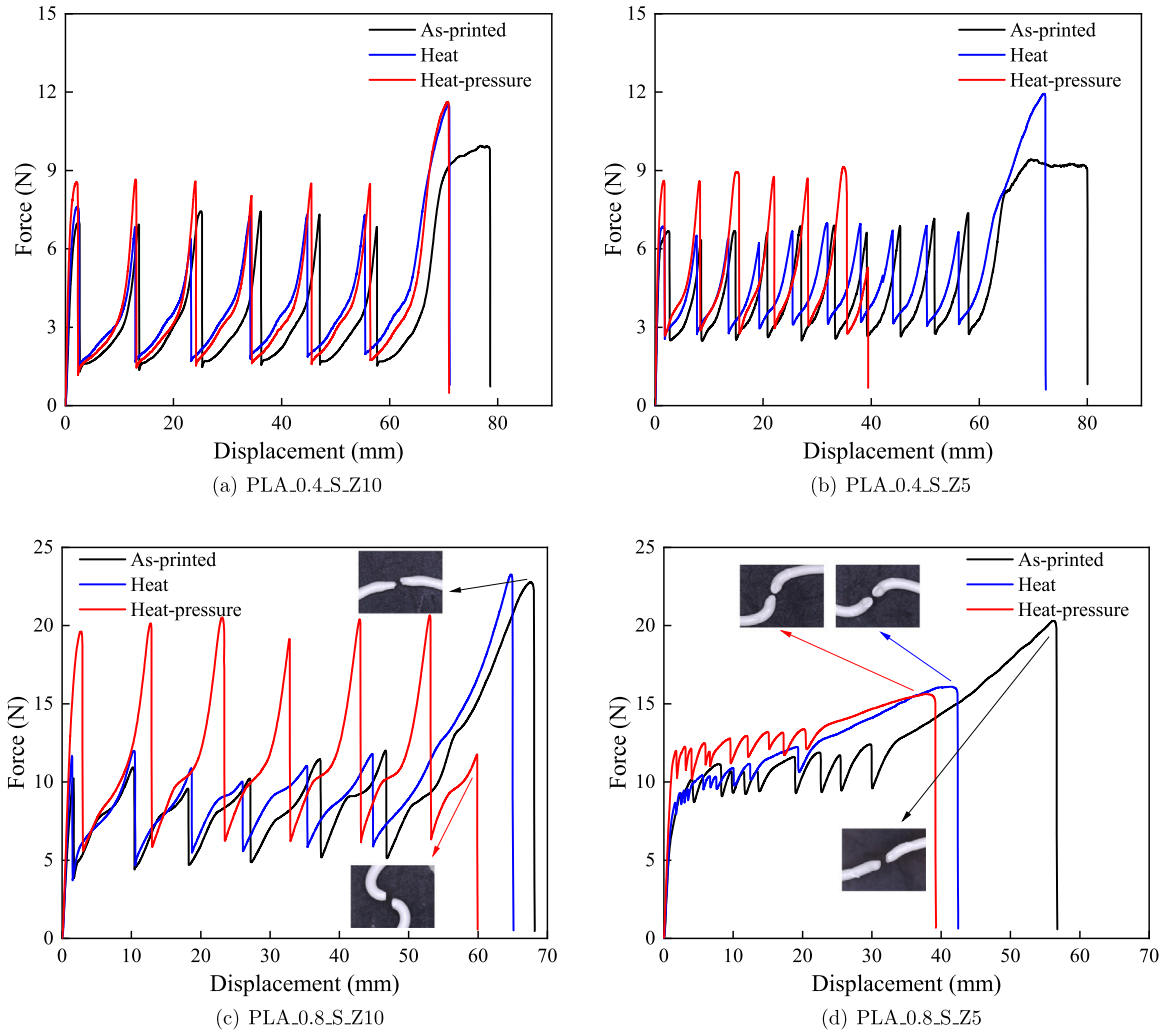

Fig. 7. Comparison of representative force-displacement tensile curves between the as-printed and post-treated single overlapping curl for (a) PLA_0.4_S_Z10, (b) PLA_0.4_S_Z5, (c) PLA_0.8_S_Z10, and (d) PLA_0.8_S_Z5. The inserted pictures show the fractured pieces of filaments.

PLA_0.4_S_Z10, Z5, and PLA_0.8_S_Z10, as shown in Fig. 7(a), 7(b), and 7(c). While the PLA_0.8_S_Z5 (in Fig. 7(d)) shows different failure modes. The as-printed OC can be fully straightened until the filament breaks at the middle position of the curl. While the heated ones break much earlier at the top or near the middle position of the curl, as observed from the inserted pictures in Fig. 7(d), possibly due to bending and/or torsion failures. The PLA_0.8_S_Z5 heated samples break before the complete hidden length unfolds resulting in a lower F_u.

After heat-pressure treatment, F_{sb} exhibits a noticeable improvement but F_u decreases. As highlighted in the inserted photos in Fig. 7(c) and 7(d), after heat and pressure the samples with thicker nozzle diameter (PLA_0.8_S_Z5 and PLA_0.8_S_Z10) break before complete unfolding of the hidden lengths resulting in lower F_u. However, the PLA_0.4_S_Z10 (Fig. 7(a)) is an exception, where the hidden length can still fully unfold and F_u is higher. This is owing to the thinner filament and bigger curl size in this structure, possibly leading to less stress concentration in the curl, preventing premature failure.

Fig. 8 shows the force-displacement curves of the PLA overlapping curls with double orientation (D). After heat and heat-pressure treatments, the samples with thinner nozzle size (0.4 mm) some of the sacrificial bonds can still break in PLA_0.4_D_Z10 and PLA_0.4_D_Z5 (Fig. 8(a) and 8(b)) and F_{sb} shows an increasing trend. Nevertheless, as discussed in Section 3.3.1, the double orientation overlapping curls tend to experience premature failure and this phenomenon is aggravated after post-treatments, where only limited sacrificial bonds can break. Due to the premature failure of the as-printed and post-treated PLA double-orientation overlapping curls, it was decided to focus the analysis further on the single-orientation overlapping curl topologies.

To further understand the increase of F_{sb} after post-treatments, Fig. 9(a) compares F_{sb} against the C_A of as-printed with heat and heat-pressure PLA overlapping curl. We see that neither C_A nor its corresponding F_{sb} change significantly after heat treatment. Therefore, it can be concluded that the heat treatment alone has negligible effects on F_{sb}. While the heat-pressure treatment improves F_{sb} and the corresponding C_A. Under the heat and pressure, the upper filament squeezes the bottom filament in the sacrificial bonds which results in the bigger C_A value. The increase in contact area explicitly increases the contact and adhesion between the upper and bottom filaments at the sacrificial bonds, resulting in an increased F_{sb} - for example, after heat-pressure PLA_0.8_S_Z10 F_{sb} increases 77 % with a corresponding C_A increase of 54 %.

Fig. 9(c) shows schematics and X-ray CT images of the various configurations of overlapping curl structures to further analyse the increase of C_A. Comparing the different configurations, the inclined angle α of PLA_0.4_S_Z10 is relatively small, the upper and bottom filaments are already closely contacting each other before treatment. After heat-pressure, the slight decrease in α limits the variation of l and consequently restrains the increase in C_A. While in PLA_0.8_S_Z10, the α value decreases significantly as the upper filament is compressed, leading to a greater rise in l (also C_A) and the corresponding increase in F_{sb}. Be-

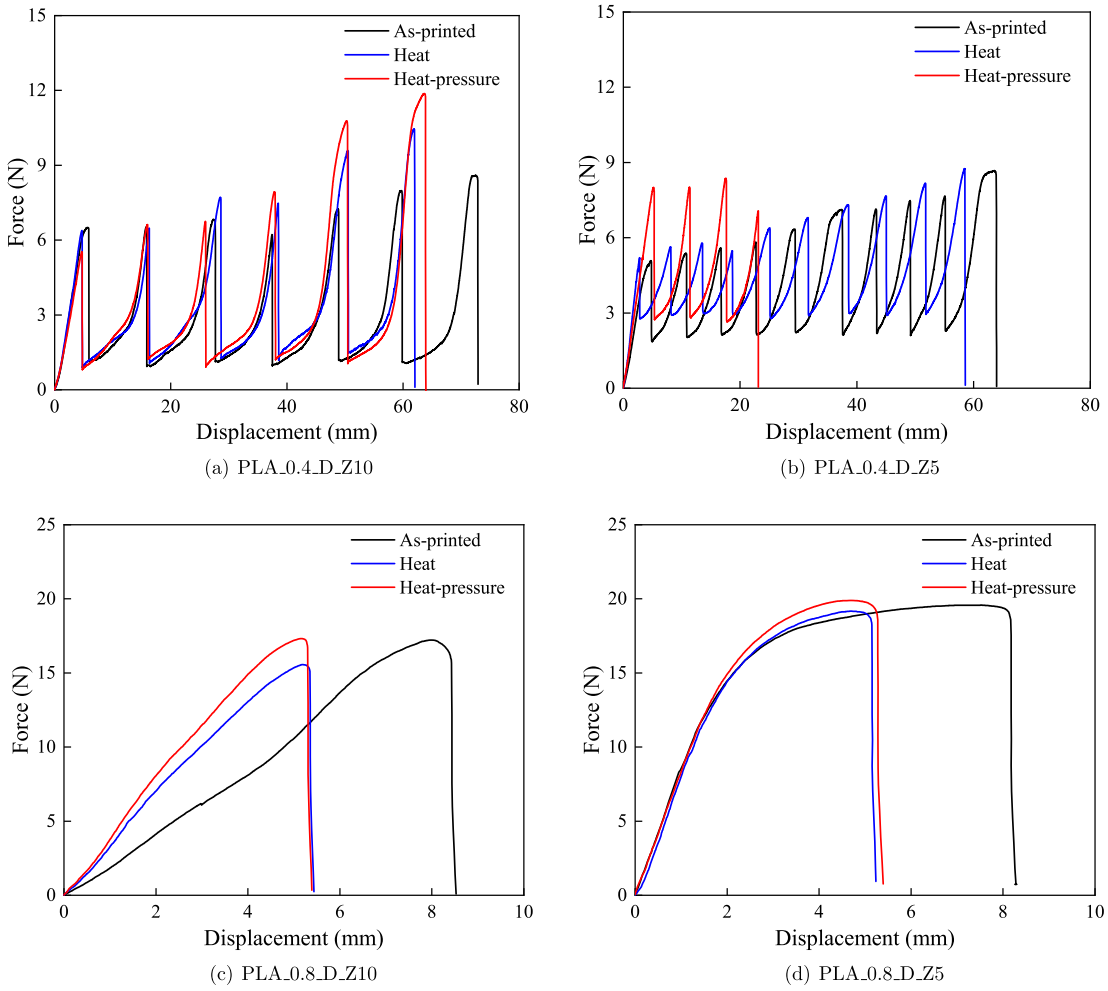

Fig. 8. Comparison of representative force-displacement tensile curves between the as-printed and post-treated double overlapping curl for (a) PLA_0.4_D_Z10, (b) PLA_0.4_D_Z5, (c) PLA_0.8_D_Z10, and (d) PLA_0.8_D_Z5.

sides, PLA_0.8_S_Z5 also shows less C_A and F_{sb} increase percentages than PLA_0.8_S_Z10. The PLA_0.8_S_Z5, featuring a smaller curl's size (2.0 mm) in comparison to the 3.6 mm of PLA_0.8_S_Z10, and hence is stiffer, resisting more to the bending of the upper filament under pressure. Therefore, after heat-pressure, we observe a slight decrease in α and alteration of l from Fig. 9(c)(ii), leading to the minor increase in C_A and F_{sb}.

3.3.3. *Sacrificial bond load-capacity effect on ultimate maximal load and toughness*

To further clarify the effect of the increase in F_{sb} on the PLA single overlapping curl mechanical response, the correlation between F_{sb} and F_u, as well as F_{sb} and E_T, are examined in Fig. 10. Based on Fig. 10(a), F_u decreases with the increasing F_{sb}. After heat-pressure, the stress concentration in the sacrificial bonds becomes severe. Besides, with F_{sb} increasing and its value approaching F_u, the break of sacrificial bonds can result in damage to the overall overlapping curl filament. Also, the defects left in the filament after the sacrificial bond breaks are more severe and more susceptible to fracture. These reasons elucidate the premature failure in the heat-pressure OC (e.g., PLA_0.8_S_Z10), where the failure mode changes from axial failure to bending and torsion failure after heat-pressure. Consistent with the analysis in Fig. 7(c) and 7(d), such failure mode transition causes incomplete hidden length, leading to the decreased F_u.

Fig. 10(b) exhibits a declining trend of E_T with the improved F_{sb} after heat-pressure treatment. By comparing the overlapping curl structures and the corresponding straight lines, it is found that the main improved toughness of OC is from the sacrificial bond break and hidden length unfolding, as also revealed in the previous findings from [25]. Even though the improved F_{sb} can contribute to increasing E_T, the ultimate toughness is still reduced by losing energy dissipation due to the reduced number of broken sacrificial bonds and incomplete unfolding of the curls. As a summary, although F_{sb} increases after heat and pressure of the PLA overlapping curls structure, the F_u and E_T decline because of the premature failure.

3.4. *Mechanical response comparison of overlapping curl manufactured by different polymeric materials*

3.4.1. *Hidden length unfolding percentage*

To understand the effects of material properties on the mechanical response of the overlapping curl structure, specimens manufactured with LCP and PA6 materials were tested and compared with the PLA results. Fig. 11 shows the force-displacement curves and average unfolding percentages p of the three materials for the topology of single orientation curl (S), 5 mm nozzle height (Z5) and two nozzle sizes 0.4 mm and 0.8 mm. The thinner nozzle size of 0.4 mm shows a 99 % unfolding percentage, while this percentage is reduced for the thicker 0.8 mm. Namely, LCP material shows only a 46.8 % unfolding percentage for the thicker nozzle, i.e., a considerable amount of hidden lengths remains in a curl shape after the sacrificial bond break, as shown in the attached snapshots. The resistance to the unfolding of the LCP_0.8_S_Z5 comes from the remarkably high Young's modulus of LCP material (5820 MPa – see Table 3), which is more than twice the value for the PLA and PA6.

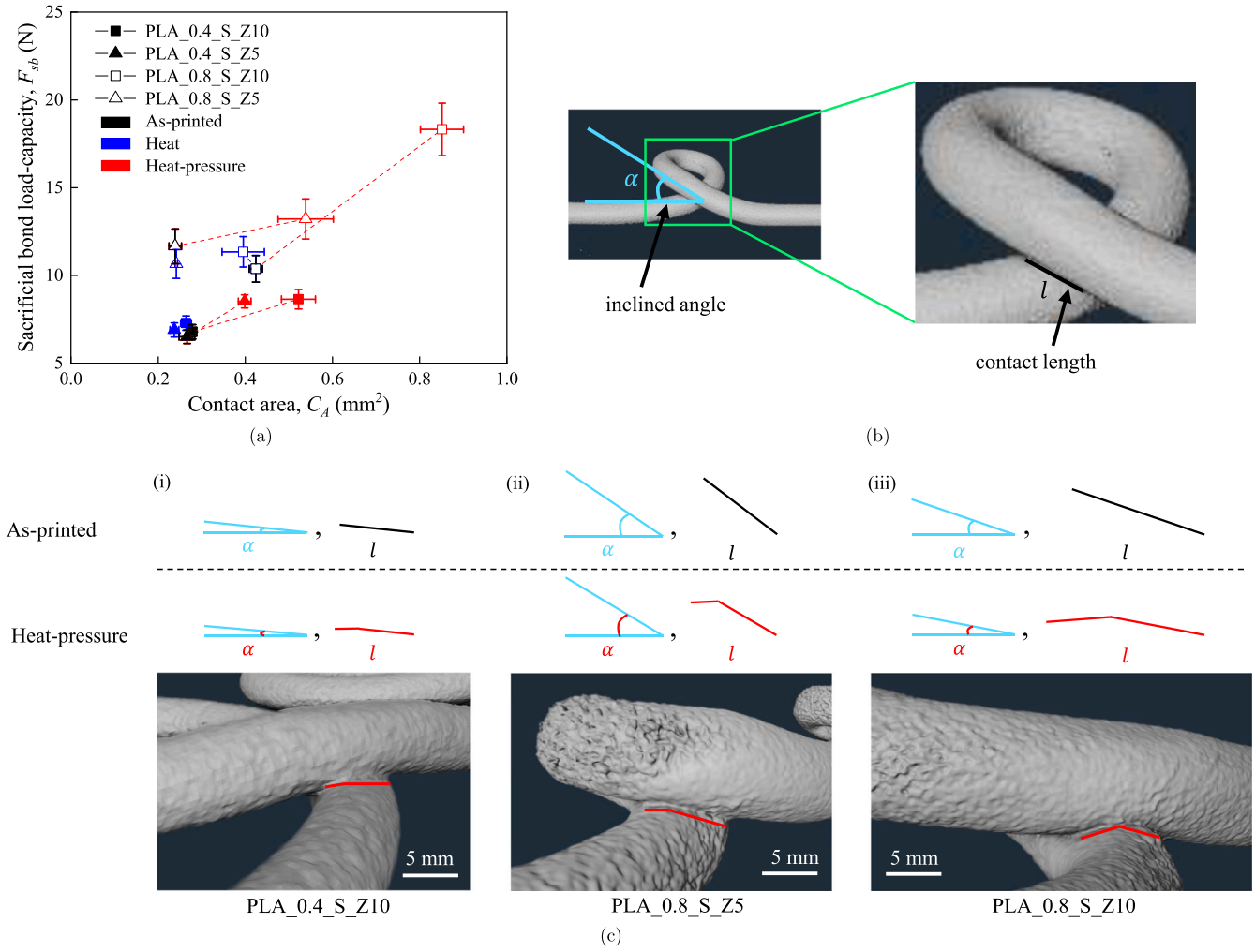

Fig. 9. (a) F_{sb} vs C_A of PLA overlapping curl before and after post-treatments. (b) The sacrificial bond structure obtained through X-ray CT. The inclined angle between the upper and bottom filaments is represented as α. The intersection of external contour of upper and bottom filaments is referred as contact length, l. (c) The schematics of (i) PLA_0.4_S_Z10, (ii) PLA_0.8_S_Z5, (iii) PLA_0.8_S_Z10 before and after heat-pressure treatment and corresponding X-ray CT images after heat-pressure treatment. The red lines highlight the change in α and l after the heat-pressure treatment.

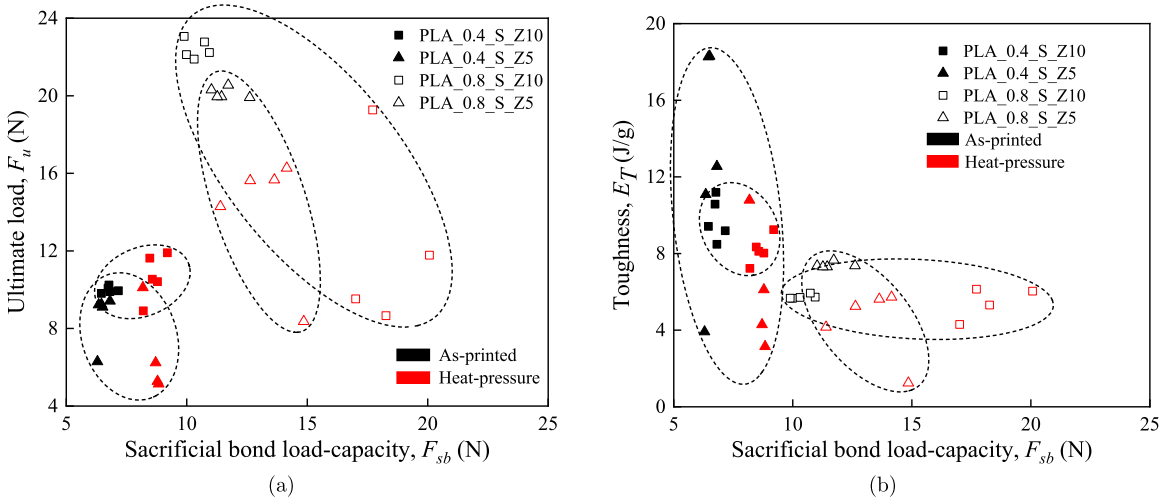

Fig. 10. (a) F_{sb} vs F_u, (b) F_{sb} vs E_T in the single as-printed and heat-pressure PLA overlapping curl. Each ellipse groups the experiment data points of one overlapping curl structure. The larger deviation in data points of F_u and E_T after heat-pressure treatment is due to different overlapping curl failure modes [26], the dashed circle captures the scattering points and indicates the trend of data evolution.

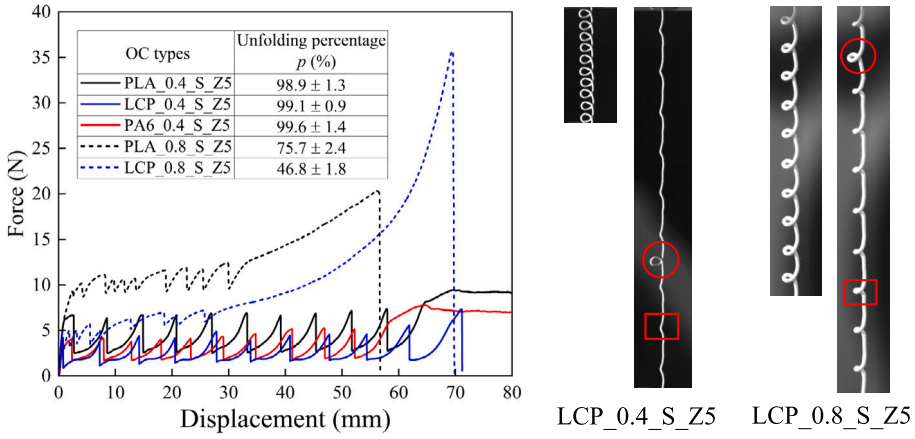

Fig. 11. Representative force-displacement curves and average hidden length unfolding percentages of overlapping curls manufactured with PLA, LCP, and PA6. The images are the captured tensile process of LCP OC when the first and last sacrificial bonds break. The red circle indicates the last sacrificial bond breaks and the rectangle highlights the remaining hidden length in the cusp at this point.

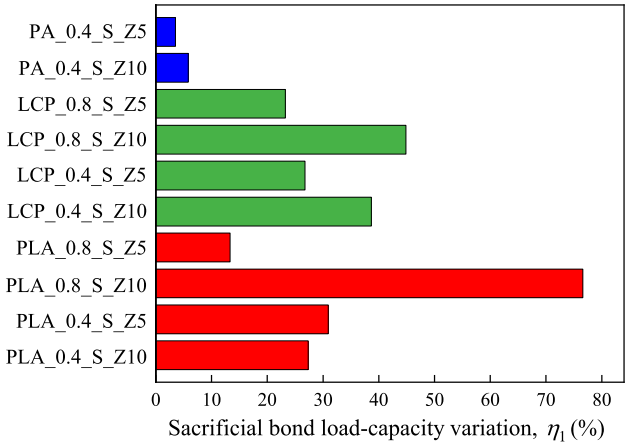

Fig. 12. Comparison of sacrificial bond load-capacity variation of overlapping curl manufactured by PLA, LCP, and PA6 materials.

As the overlapping curl filament diameter increases, a higher sacrificial bond load-capacity is required to stretch the curl before the last sacrificial bond breaks, which can be roughly estimated from the tensile deformation in the OC filament segment. From Fig. 11, LCP_0.8_S_Z5 has a lower sacrificial bond load-capacity compared to PLA_0.8_S_Z5, leading to earlier sacrificial bond failure. In other words, the sacrificial bonds in LCP_0.8_S_Z5 break before the hidden length fully unfolds, resulting in the lowest unfolding percentage.

3.4.2. Sacrificial bond load-capacity

We also applied heat-pressure treatment to the LCP and PA6 single overlapping curl, aiming to improve the sacrificial bond load-capacity and toughness. The average F_{sb} variation η_1 before and after heat-pressure, is defined as:

$$\eta_1 = \frac{\overline{F}_{sb}^{\text{heat-pressure}} - \overline{F}_{sb}^{\text{as-printed}}}{\overline{F}_{sb}^{\text{as-printed}}} \tag{4}$$

where $\overline{F}_{sb}^{\text{as-printed}}$ and $\overline{F}_{sb}^{\text{heat-pressure}}$ are the average F_{sb} values for each overlapping curl structure before and after heat-pressure treatment.

In Fig. 12, the F_{sb} of PLA and LCP overlapping curls exhibit a significant increase after heat-pressure, while PA6 samples show little improvement. In order to better understand these differences, Fig. 13 shows SEM images of the sacrificial bond fracture surfaces of as-printed and after heat-pressure of the three materials. The contact area of the as-printed surfaces is highlighted by the red dashed ellipses. After heat-pressure, by comparing the morphology of the fracture surfaces, we could estimate the original contact area contour highlighted in red and the contact area after heat-pressure highlighted by blue dashed ellipses. It is clear that the contact area in the sacrificial bond increases in the heat-pressure for the PLA sample - PLA_0.8_S_Z10. Besides, the fracture surface is rough, especially in the zoomed area Fig. 13(a)(iii), indicating a good adhesion, which results in more energy dissipation during the sacrificial bond break. While in Fig. 13(b), the heat-pressure LCP sample - LCP_0.8_S_Z10, has a glossy and smooth fracture surface throughout the sacrificial bond. Although the contact area increases after heat-pressure, the adhesion between the upper and bottom filaments is low. The rougher fracture surface after heat-pressure on the PLA sample also explains its larger increase of 77 % F_{sb} than after heat-pressure on the LCP sample, with an increase of 46 %. From the fracture surfaces of the PA sample - PA6_0.4_S_Z5 in Fig. 13(c), the contact area does not change significantly after heat-pressure. This could be attributed to the mechanical resilience of PA6 material [51,52]. After heat-pressure, the upper filament possibly springs back and the sacrificial bond recovers its original geometry shape, corresponding to the little F_{sb} improvement.

3.4.3. Toughness variation

Similarly to the variation of the F_{sb}, the average variation of the toughness E_T is defined as η_2 before and after heat-pressure, as follows:

$$\eta_2 = \frac{\overline{E}_T^{\text{heat-pressure}} - \overline{E}_T^{\text{as-printed}}}{\overline{E}_T^{\text{as-printed}}} \tag{5}$$

where $\overline{E}_T^{\text{as-printed}}$ and $\overline{E}_T^{\text{heat-pressure}}$ represent the average toughness values for each overlapping curl structure before and after heat-pressure treatment.

Fig. 14 shows the toughness variation values η_2 of PLA, LCP, and PA6 overlapping curls and are compared according to their basic material properties. The PLA overlapping curls present a negative η_2 (−67 % to −5 %) while LCP samples show a positive η_2 value ranging from + 12 % to + 32 %. The fracture strain levels for PLA and LCP are similar (0.033 and 0.15), we then compare η_2 with respect to their fracture strengths (54 MPa and 311 MPa). The high fracture strength of LCP makes the filament withstand higher stress concentration and possible defects from the sacrificial bonds break, avoiding premature failure of the OC structure and, hence, increasing the toughness after heat-pressure. On the other hand, PLA and PA6 exhibit comparable fracture strengths (54 MPa and 47 MPa), but there is a pronounced discrepancy in the fracture strain, 0.033 and >2, respectively. In Fig. 14, PA6 material shows a cumulative toughness: + 37 % to + 46 %. The exceptionally high fracture strain of PA6 material guarantees the PA6 overlapping curl structure to

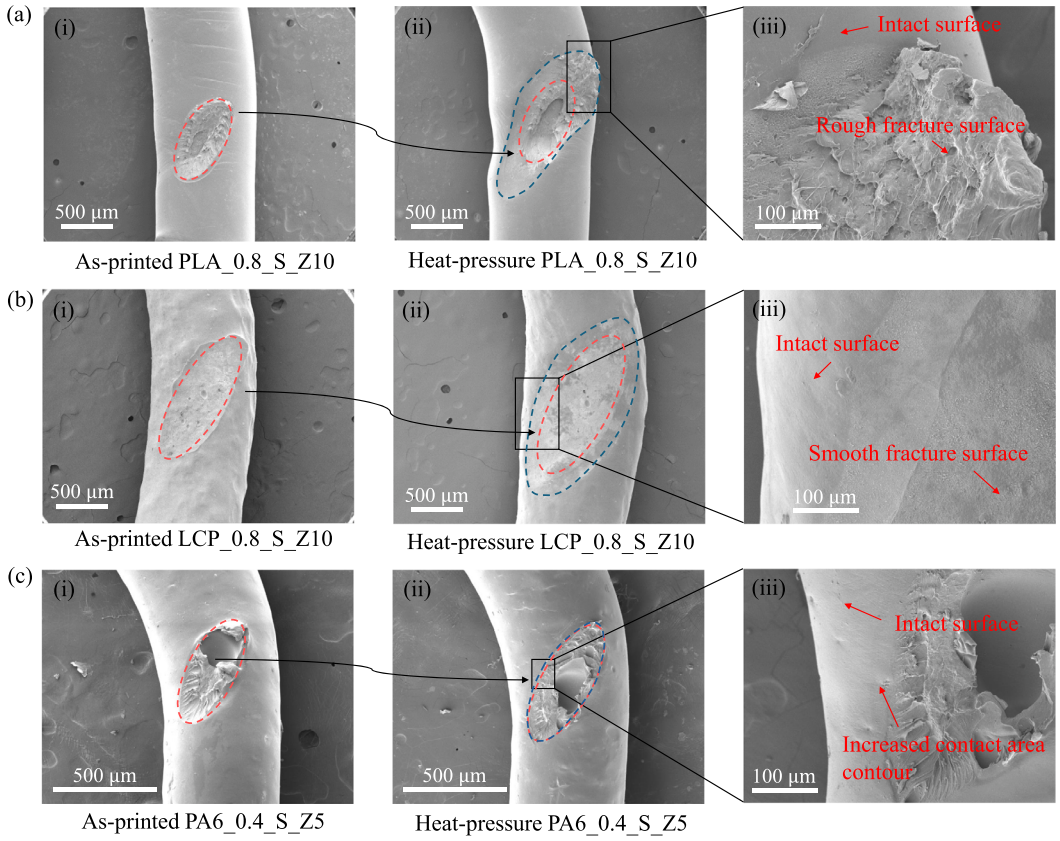

Fig. 13. Fracture surfaces observed under SEM of (a) PLA_0.8_S_Z10, (b) LCP_0.8_S_Z10, and (c) PA6_0.4_S_Z5. The red dashed ellipses depict the original contact contour. The blue dashed ellipses outline the contact contour after heat-pressure treatment.

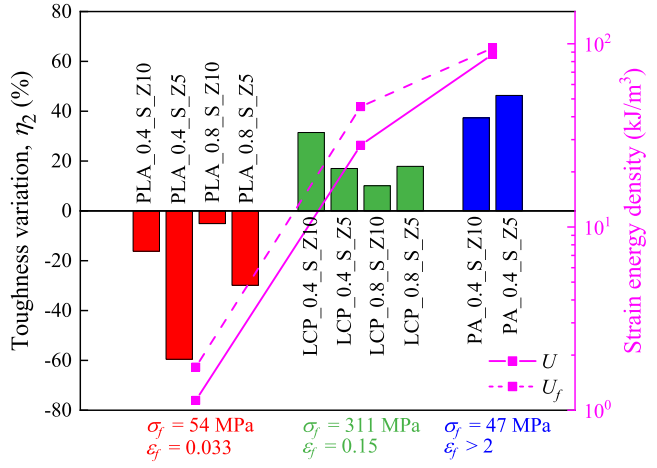

Fig. 14. Comparison of the toughness variation of overlapping curl manufactured by PLA, LCP, and PA6 materials. The σ_f and ϵ_f are the material fracture strength and fracture strain - see Table 3. ϵ_f of PA6 is chosen as 2 for calculating U and U_f.

fully unfold with increased ultimate load after heat-pressure, leading to improved toughness.

To enhance the toughness by heat-pressure treatment, a recommendation towards the material selection to manufacture overlapping curl structure is proposed here. We relate η_2 with the material constitutive parameters. The strain energy density measures the amount of energy absorbed or stored per unit volume in a material owing to deformation, defined by the area underneath the strain-stress curve [53],

$$U = \int \sigma(\epsilon)\, d\epsilon \tag{6}$$

In approximation to strain energy density, we define a parameter U_f considering the fracture strength σ_f and fracture strain ϵ_f,

$$U_f = \sigma_f \cdot \epsilon_f \tag{7}$$

The line plots in Fig. 14 compare η_2 of the three materials with U and U_f. η_2 undergoes a transition from negative to positive value with U increasing. Besides, the $\eta_2 - U_f$ shows the same positive correlation as $\eta_2 - U$. From the relationship between η_2 and U_f, rather than obtaining the complete stress-strain curve to determine U, one can directly check the fracture strength and fracture strain to make an initial selection of the printing material on the design space. In this case, setting PLA material as baseline, the printing material with a larger U_f value promises an improved toughness after heat-pressure treatment on the overlapping curl structure. The hidden lengths extension and toughness of overlapping curl are considered as important mechanical properties that can be applied in many areas such as strain sensors [54] and energy dissipation reinforcement [12,14]. In future research, the parameters such as temperature and pressure during the heat-pressure treatment could be optimized to reach the best combination of F_{sb}, F_u, and E_T to meet the diverse requirements of devices.

4. Conclusions

The as-printed PLA overlapping curl tensile test revealed the full unfolding of the hidden lengths in the single orientation curls, whereas premature failure occurred in the double orientations ones due to the greater stress concentration caused by its larger extruded filament orbit curvature. The heat treatment alone had negligible effects on the sacrificial bond load-capacity. While, after heat-pressure treatment, the sacrificial bond load-capacity increased because of the increased contact area. In particular, there was a 77 % enhancement in sacrificial bond load-capacity of PLA overlapping curl with 0.8 mm thick nozzle,

single orientation, and 10 mm nozzle height (PLA_0.8_S_Z10) and the corresponding contact area increased by 54 %. However, the enhanced sacrificial bond load-capacity introduced defects into the overlapping curl filament after the sacrificial bonds break. As a result, the hidden lengths exhibited less unravelling, and both ultimate load and toughness decreased owing to premature failure. In contrast, after heat-pressure, the LCP and PA6 overlapping curl structures demonstrated an improved toughness. A high fracture strength (e.g., LCP, 311 MPa) or a high fracture strain (e.g., PA6, >2) of the material can ensure the hidden length unfolding after heat-pressure, leading to improved toughness. Based on this, we can conclude that the heat and pressure post-treatment can improve the OC toughness as long as the complete unfolding of hidden length is guaranteed. Materials with high fracture strength or high fracture strain have proven to be more robust against the defect imposed by the post-treatment avoiding premature failure and guaranteeing a complete unfolding. The choice of materials is therefore critical for enhancing the OC toughness.

CRediT authorship contribution statement

Zhiyuan Xu: Writing – original draft, Methodology, Formal analysis, Data curation, Conceptualization. **Ran Tao:** Writing – review & editing, Visualization, Validation, Supervision, Methodology, Formal analysis, Conceptualization. **Kunal Masania:** Writing – review & editing, Supervision, Conceptualization. **Sofia Teixeira de Freitas:** Writing – review & editing, Visualization, Validation, Supervision, Methodology, Funding acquisition, Conceptualization.

Declaration of competing interest

The authors declare the following financial interests/personal relationships which may be considered as potential competing interests: Zhiyuan Xu reports financial support was provided by Chinese Scholarship Council. Sofia Teixeira de Freitas reports financial support was provided by Foundation for Science and Technology. If there are other authors, they declare that they have no known competing financial interests or personal relationships that could have appeared to influence the work reported in this paper.

Acknowledgements

The authors gratefully acknowledge the financial support from the China Scholarship Council (No. CSC202107720061). This work is also supported by FCT, through IDMEC, under LAETA, project UIDB/50022/2020.

Data availability

The data is available on the DOI: https://doi.org/10.4121/5df63ddf-8630-4a05-b446-75dd9abe3e24.

References

[1] I. Su, M.J. Buehler, Nanomechanics of silk: the fundamentals of a strong, tough and versatile material, Nanotechnology 27 (30) (2016) 302001.
[2] A. Nova, S. Keten, N. Pugno, A. Redaelli, M. Buehler, Molecular and nanostructural mechanisms of deformation, strength and toughness of spider silk fibrils, Nature Precedings (2010) 1.
[3] G.E. Fantner, T. Hassenkam, J.H. Kindt, J.C. Weaver, H. Birkedal, L. Pechenik, J.A. Cutroni, G.A. Cidade, G.D. Stucky, D.E. Morse, et al., Sacrificial bonds and hidden length dissipate energy as mineralized fibrils separate during bone fracture, Nat. Mater. 4 (8) (2005) 612–616.
[4] B. Vagaská, L. Bačáková, E. Filovaá, K. Balík, Osteogenic cells on bio-inspired materials for bone tissue engineering, Physiol. Res. 59 (3) (2010).
[5] B.L. Smith, T.E. Schäffer, M. Viani, J.B. Thompson, N.A. Frederick, J. Kindt, A. Belcher, G.D. Stucky, D.E. Morse, P.K. Hansma, Molecular mechanistic origin of the toughness of natural adhesives, fibres and composites, Nature 399 (6738) (1999) 761–763.
[6] Z. Yin, F. Hannard, F. Barthelat, Impact-resistant nacre-like transparent materials, Science 364 (6447) (2019) 1260–1263.
[7] F. Narducci, S. Pinho, Exploiting nacre-inspired crack deflection mechanisms in cfrp via micro-structural design, Compos. Sci. Technol. 153 (2017) 178–189.
[8] A. Wagih, R. Tao, G. Lubineau, Bio-inspired adhesive joint with improved interlaminar fracture toughness, Composites, Part A, Appl. Sci. Manuf. 149 (2021) 106530.
[9] M.E. Kazemi, V. Medeau, Y. Chen, Z. Xu, N. Petrinic, E. Greenhalgh, P. Robinson, J. Finlayson, S.T. Pinho, Ballistic performance of bio-inspired hybrid interleaved composite structures suitable for aerospace applications, Composites, Part A, Appl. Sci. Manuf. 179 (2024) 107992.
[10] F. Zhu, L. Cheng, Z.J. Wang, W. Hong, Z.L. Wu, J. Yin, J. Qian, Q. Zheng, 3d-printed ultratough hydrogel structures with titin-like domains, ACS Appl. Mater. Interfaces 9 (13) (2017) 11363–11367.
[11] I. Hussain, S.M. Sayed, S. Liu, O. Oderinde, F. Yao, G. Fu, Glycogen-based self-healing hydrogels with ultra-stretchable, flexible, and enhanced mechanical properties via sacrificial bond interactions, Int. J. Biol. Macromol. 117 (2018) 648–658.
[12] S. Zou, D. Therriault, F.P. Gosselin, Toughening elastomers via microstructured thermoplastic fibers with sacrificial bonds and hidden lengths, Extreme Mechanics Letters 43 (2021) 101208.
[13] E. Ducrot, Y. Chen, M. Bulters, R.P. Sijbesma, C. Creton, Toughening elastomers with sacrificial bonds and watching them break, Science 344 (6180) (2014) 186–189.
[14] S. Zou, D. Therriault, F.P. Gosselin, Spiderweb-inspired, transparent, impact-absorbing composite, Cell Reports Physical Science 1 (11) (2020).
[15] M.J. Palmeri, K.W. Putz, L.C. Brinson, Sacrificial bonds in stacked-cup carbon nanofibers: biomimetic toughening mechanisms for composite systems, ACS Nano 4 (7) (2010) 4256–4264.
[16] N. Li, J. Huang, Y. Wang, L. Xiao, P. Fu, H. Yu, X. Nie, J. Jiang, Y. Zhu, Z. Guo, Simultaneously strengthening, toughening, and conductivity improving for epoxy at ultralow carbonaceous filler content by constructing 3d nanostructures and sacrificial bonds, Composites, Part A, Appl. Sci. Manuf. 137 (2020) 106014.
[17] D. Rahmatabadi, M. Khajepour, A. Bayati, K. Mirasadi, M.A. Yousefi, A. Shegeft, I. Ghasemi, M. Baniassadi, K. Abrinia, M. Bodaghi, et al., Advancing sustainable shape memory polymers through 4d printing of polylactic acid-polybutylene adipate terephthalate blends, Eur. Polym. J. 216 (2024) 113289.
[18] D. Rahmatabadi, I. Ghasemi, M. Baniassadi, K. Abrinia, M. Baghani, 3d printing of pla-tpu with different component ratios: fracture toughness, mechanical properties, and morphology, Journal of Materials Research and Technology 21 (2022) 3970–3981.
[19] I. Khan, I. Barsoum, M. Abas, A. Al Rashid, M. Koç, M. Tariq, A review of extrusion-based additive manufacturing of multi-materials-based polymeric laminated structures, Compos. Struct. (2024) 118490.
[20] D. Rahmatabadi, A. Bayati, M. Khajepour, K. Mirasadi, I. Ghasemi, M. Baniassadi, K. Abrinia, M. Bodaghi, M. Baghani, Poly (ethylene terephthalate) glycol/carbon black composites for 4d printing, Mater. Chem. Phys. 325 (2024) 129737.
[21] D. Rahmatabadi, K. Soltanmohammadi, M. Aberoumand, E. Soleyman, I. Ghasemi, M. Baniassadi, K. Abrinia, M. Bodaghi, M. Baghani, 4d printing of porous pla-tpu structures: effect of applied deformation, loading mode and infill pattern on the shape memory performance, Phys. Scr. 99 (2) (2024) 025013.
[22] I. Liashenko, A. Hrynevich, P.D. Dalton, Designing outside the box: unlocking the geometric freedom of melt electrowriting using microscale layer shifting, Adv. Mater. 32 (28) (2020) 2001874.
[23] J. Tian, J. Li, A. Sauret, T. Kong, X. Wu, Y. Lu, H.C. Shum, Facile control of liquid-rope coiling with tunable electric field configuration, Phys. Rev. Appl. 12 (1) (2019) 014034.
[24] H. Yuk, X. Zhao, A new 3d printing strategy by harnessing deformation, instability, and fracture of viscoelastic inks, Adv. Mater. 30 (6) (2018) 1704028.
[25] R. Passieux, L. Guthrie, S.H. Rad, M. Lévesque, D. Therriault, F.P. Gosselin, Instability-assisted direct writing of microstructured fibers featuring sacrificial bonds, Adv. Mater. 27 (24) (2015) 3676–3680.
[26] S. Zou, D. Therriault, F. Dé, R.P. Gosselin, Failure mechanisms of coiling fibers with sacrificial bonds made by instability-assisted fused deposition modeling, Soft Matter 14 (2018) 9777.
[27] N. Willemstein, H. van der Kooij, A. Sadeghi, 3d printing of soft fluidic actuators with graded porosity, Soft Matter 18 (38) (2022) 7269–7279.
[28] D. Ma, X. Tian, J. Han, L. Xia, Modeling for silicone foam material extrusion with liquid rope coiling, Int. J. Mech. Sci. 249 (2023) 108234.
[29] A. Davoudinejad, M.R. Khosravani, D.B. Pedersen, G. Tosello, Influence of thermal ageing on the fracture and lifetime of additively manufactured mold inserts, Eng. Fail. Anal. 115 (2020) 104694.
[30] M.R. Khosravani, D. Anders, T. Reinicke, Effects of post-processing on the fracture behavior of surface-treated 3d-printed parts, CIRP Journal of Manufacturing Science and Technology 46 (2023) 148–156.
[31] P.-T. Brun, C. Inamura, D. Lizardo, G. Franchin, M. Stern, P. Houk, N. Oxman, The Molten glass sewing machine, Philos. Trans. A Math. Phys. Eng. Sci. 375 (2093) (2017) 20160156.
[32] M. Zhang, J. Zhang, D. Yang, Y. Li, X. Cui, K. Fu, Improved interlayer performance of short carbon fiber reinforced composites with bio-inspired structured interfaces, Addit. Manuf. 79 (2024) 103936.
[33] G. Barnes, R. Woodcock, Liquid rope-coil effect, Am. J. Phys. 26 (4) (1958) 205–209.
[34] N.M. Ribe, M. Habibi, D. Bonn, Liquid rope coiling, Annu. Rev. Fluid Mech. 44 (2012) 249–266.

[35] P.-T. Brun, B. Audoly, N.M. Ribe, T.S. Eaves, J.R. Lister, Liquid ropes: a geometrical model for thin viscous jet instabilities, Phys. Rev. Lett. 114 (2015) 174501.
[36] Y. Zhou, Y. Dong, X. Li, J. Li, S.Q. Shi, J. Li, J. Luo, Spider silk inspired robust and photoluminescent soybean-protein-based materials, Macromol. Mater. Eng. 306 (8) (2021) 2100155.
[37] J. Li, S. Li, J. Huang, A.Q. Khan, B. An, X. Zhou, Z. Liu, M. Zhu, Spider silk-inspired artificial fibers, Adv. Sci. 9 (5) (2022) 2103965.
[38] T.L. Bergman, A.S. Lavine, F.P. Incropera, D.P. DeWitt, Introduction to Heat Transfer, John Wiley & Sons, 2011.
[39] Formfutura BV company, Technical Datasheet, ReForm™ - rPLA, https://www.formfutura.com.
[40] USA Ticona Co., Ltd, Technical Datasheet, Vectra®A950 - LCP (2022), https://www.campusplastics.com.
[41] Fiberthree GmbH company, Technical Datasheet, F3 PA Pure Pro (2019), https://www.fiberthree.com.
[42] L. Song, Y. Li, X. Meng, T. Wang, Y. Shi, Y. Wang, S. Shi, L.-Z. Liu, Crystallization, structure and significantly improved mechanical properties of pla/ppc blends compatibilized with pla-ppc copolymers produced by reactions initiated with tbt or tdi, Polymers 13 (19) (2021) 3245.
[43] Proto Labs, Inc., Glass Transition Temperature (Tg) of Polymers, https://www.protolabs.com/resources/design-tips/glass-transition-temperature-of-polymers/.
[44] S. Gantenbein, K. Masania, W. Woigk, J.P. Sesseg, T.A. Tervoort, A.R. Studart, Three-dimensional printing of hierarchical liquid-crystal-polymer structures, Nature 561 (7722) (2018) 226–230.
[45] Y. Lin, Q. Shi, Y. Hao, Z. Song, Z. Zhou, Y. Fu, X. Chen, Z. Zhang, J. Wu, The effect of non-uniform pitch length and spiraling pathway on the mechanical properties of coiled carbon nanotubes, Int. J. Mech. Sci. (2023) 108532.
[46] L. Aliotta, L.M. Sciara, P. Cinelli, I. Canesi, A. Lazzeri, Improvement of the pla crystallinity and heat distortion temperature optimizing the content of nucleating agents and the injection molding cycle time, Polymers 14 (5) (2022) 977.
[47] P.A.K. Jain, S. Sattar, D. Mulqueen, D. Pedrazzoli, S. Kravchenko, O. Kravchenko, Role of annealing and isostatic compaction on mechanical properties of 3d printed short glass fiber nylon composites, Addit. Manuf. 51 (2022) 102599.
[48] Q. Meng, Y. Gu, L. Luo, S. Wang, M. Li, Z. Zhang, Annealing effect on crystalline structure and mechanical properties in long glass fiber reinforced polyamide 66, J. Appl. Polym. Sci. 134 (23) (2017).
[49] M. Song, X. Wang, R. Du, Z. Zhou, X. Li, G. Li, Y. Luo, Effects of liquid crystal polymer (lcp) on the structure and performance of peek/cf composites, RSC Adv. 12 (20) (2022) 12446–12452.
[50] N. Fleck, G. Muller, M. Ashby, J. Hutchinson, Strain gradient plasticity: theory and experiment, Acta Metall. Mater. 42 (2) (1994) 475–487.
[51] M.T. Dehkordi, H. Nosraty, M.M. Shokrieh, G. Minak, D. Ghelli, Low velocity impact properties of intra-ply hybrid composites based on basalt and nylon woven fabrics, Mater. Des. 31 (8) (2010) 3835–3844.
[52] L. Lu, Z. Li, H. He, Y. Xie, W. Wang, Bioinspired strain sensor using multiwalled carbon nanotube/polyvinyl butyral/nylon cloth for wireless sensing applications, IEEE Sens. J. 22 (13) (2022) 12664–12672.
[53] Y. Ding, K. Yu, All-strength-grade polyethylene engineered cementitious composite (pe-ecc): mechanical performance, energy parameters and its performance-based design method, in: Advances in Engineered Cementitious Composites, Elsevier, 2022, pp. 39–76.
[54] Q. Wu, S. Zou, F.P. Gosselin, D. Therriault, M.-C. Heuzey, 3d printing of a self-healing nanocomposite for stretchable sensors, J. Mater. Chem. C 6 (45) (2018) 12180–12186.